International Journal of Heat and Mass Transfer 63 (2013) 141–149

Contents lists available at SciVerse ScienceDirect

International Journal of Heat and Mass Transfer

journal homepage: www.elsevier.com/locate/ijhmt

Study of the effect of moxibustion on the blood flow

Chinlong Huang [a], Tony W.H. Sheu [a,b,c,*]

[a] Department of Engineering Science and Ocean Engineering, National Taiwan University, Taiwan, ROC
[b] Institute of Applied Mathematical Sciences, National Taiwan University, Taiwan, ROC
[c] Center for Advanced Studies in Theoretical Sciences (CASTS), National Taiwan University, Taiwan, ROC

ARTICLE INFO

Article history:
Received 7 November 2012
Received in revised form 8 January 2013
Accepted 22 March 2013
Available online 27 April 2013

Keywords:
Heat transfer
Moxibustion
Numerical simulation
Infrared

ABSTRACT

While heat transfer plays an important role in thermal therapies by moxibustion, little information is currently available in the literature. Our aim is to get the temperature distribution beneath the skin surface and reveal how an imposed heat can affect blood flow in vessels and vice versa. For a better understanding of the heat transfer process due to moxibustion, skin temperature measurement is conducted to get the skin surface temperature, which enables us to carry out a numerical simulation of heat/flow equations in human legs. Subject to the measured skin surface temperature by virtue of the calibrated real time infrared camera, the temperature beneath the heating position and the heat transfer in blood vessel are numerically obtained. When the temperature becomes higher, blood flow velocity is found to increase in this study because of the accompanying decreased viscosity. Both of the lying and standing poses are investigated in the current moxibustion study. For the lying case, the blood flow has a higher mean velocity while for the case of standing pose a larger change of the mean velocity is predicted. From the thermal energy point of view, the lying pose is a better choice because its resulting higher blood flow velocity can transfer heat more effectively to the whole body.

1. Introduction

Thermal therapy is a clinical procedure of increasing the temperature above 40 °C or even 60 °C at a properly chosen area of patients' body surface. In the past, clinicians have developed a number of ablation strategies to destruct tumor cells. Moxibustion is another widely accepted thermal therapy in Chinese medicine [1]. Human body is exposed to a high temperature by different means for a certain period of time. The resulting skin temperature can be locally raised by a sufficient amount and it can cause an apparent effect to occur. Depending on the distance between the skin and moxa, thermal injury on the skin may be resulted from temperature elevation in tissues above a threshold value, say 60 °C at most (skin surface).

It is essential to provide medical doctors with some useful information of the bioheat during therapeutic therapy since it is normally difficult for them to conduct thermal analysis. Some analytical studies have been performed, for example, by Brix et al. [2] who derived the analytic solutions by the Green's function method to estimate temperature elevation. Durkee and Antich [3] developed the transient analytic method in a multi-layer structure to get temperature distributed on the skin, muscle, and bone. A three-dimensional acoustics-thermal-fluid coupling model has been developed in [4,5] to investigate the influence of blood vessels on the temperature distribution during liver tumor ablation using the high-intensity focused ultrasound.

The body surface temperature is attributed to blood circulation beneath the skin, local metabolism between the tissues, and heat exchange between the skin and its surrounding tissues. Under the normal condition, thermal energy balance can be well maintained and leads thus to a skin temperature suitable for metabolic functions. Physiological abnormality or change in the surrounding conditions may affect the skin temperature and can even cause a net thermal flux in or out of the human body [6].

Numerical modeling is now accepted as an effective means of understanding the detailed heating process in a physiological structure. This technique also helps us to quantify the degree of thermal damage on the tissues due to an applied heat. Henriques and Moritz [7] have made some discussions on the burns under different situations. Actually, there has been a long-standing interest in getting skin thermal properties [8] to clarify under what condition thermal damage may occur. These usually involve the contact between skin and the heated object [9], in which thermal conduction and heat capacity are two dominant factors. Investigation of the bioheat transfer can be carried out to get the spatial and temporal temperature distributions. When a heat source is exposed to skin surface, its local temperature is the result of the

* Corresponding author. Address: Department of Engineering Sciences and Ocean Engineering, National Taiwan University, No. 1, Sec. 4, Roosevelt Road, Taipei 10617, Taiwan, ROC. Tel.: +886 2 33665746; fax: +886 2 23929885.
E-mail address: twhsheu@ntu.edu.tw (T.W.H. Sheu).

0017-9310/$ - see front matter © 2013 Elsevier Ltd. All rights reserved.
http://dx.doi.org/10.1016/j.ijheatmasstransfer.2013.03.057

Nomenclature

C_p	specific heat
g	gravity
h	enthalpy
i	internal energy
k	thermal conductivity
p	static pressure
T	temperature
t	time
V_{mean}	mean velocity
W_b	perfusion rate for tissue
$\vec{V}$	velocity vector
u, v, w	velocity components
x, y, z	Cartesian coordinates
$\underline{q}$	energy flux

Greek symbols

ρ	density of calf
ρ_b	density of blood
$\underline{J}$	viscous stress tensor
$\bar{\bar{\mu}}$	viscosity

thermal energy balance between the heat conduction and the heat convection in blood flow motion. Anderson and Burnside [10] measured the blood perfusion effect using a spatial sinusoidal heating by ultrasound. Perfusion was normally simulated by solving the Pennes equation.

In the present study, our attention is focused on the heat transfer process and the blood perfusion for an externally applied heat to the calf, shown in Fig. 1, by moxibustion. In Chinese medicine, the acupoint in gall bladder (GB) meridian has direct relevance to hemicrania and joint ache. At the calf section, the number of capillaries near the GB acupoints is much greater than those found at other parts of the body [11]. The distances between the acupoints GB37-GB38 and GB38-GB39 are about an inch. Therefore, the acupoint GB38 has been the focus of our previous investigations [12–14]. The axial image of the right leg for the GB38 acupoint [15] is shown in Fig. 2, which contains the anterior tibia, posterior tibia, peroneal, and some superficial vessels. In the present simulation of heat transfer around the location GB38, the effect of blood flow in two superficial peroneal veins, which are closest to the heating location, will be taken into account.

The rest of this paper is organized as follows. The infrared (IR) camera employed in the surface temperature measurement and the numerical method performed to get the interior temperature will be briefly described in the next section. This is followed by comparing the temperatures, due to moxibustion, obtained from the experimental calibration and the numerical simulation. Finally, a summary of the present study is drawn.

2. Working equations and numerical method

To simulate the moxibustion process, the governing equations for tissues beneath the skin of leg schematic in Fig. 1 and the Newtonian flow in blood vessels are given below for the respective mass, momentum, and energy conservations:

$$\nabla \cdot \underline{u} = 0, \tag{1}$$

$$\underline{u}_t + \underline{u} \cdot \nabla \underline{u} = -\frac{1}{\rho}\nabla p + \frac{1}{\rho}\nabla \cdot \underline{\underline{\tau}}, \tag{2}$$

$$h_t + \underline{u} \cdot \nabla h = \frac{1}{\rho}\nabla \cdot \underline{q} + \frac{1}{\rho}\underline{\underline{\tau}} \cdot \nabla \underline{\tau} + \frac{1}{\rho}\frac{dp}{dt}, \tag{3}$$

In the hemodynamic equations (1) and (2), p is the density of the blood fluid, $\underline{u}$ is the blood flow velocity vecter, p is the blood flow pressure, and $\underline{\underline{\tau}}$ is the shear stress tensor defined as $\underline{\underline{\tau}} = \mu(\nabla \underline{u} + \nabla \underline{u}^T)$ where $\mu(T)\left(\equiv \mu(T = 37\,^\circ\mathrm{C})\left(1 - 4\frac{T-37}{T+273}\right)\right)$ is denoted as the blood viscosity [16]. To simplify the analysis, viscoelastic effect in the blood flow is not taken into account in the current study. In the energy equation (3) for blood flow, $h(\equiv C_p T)$

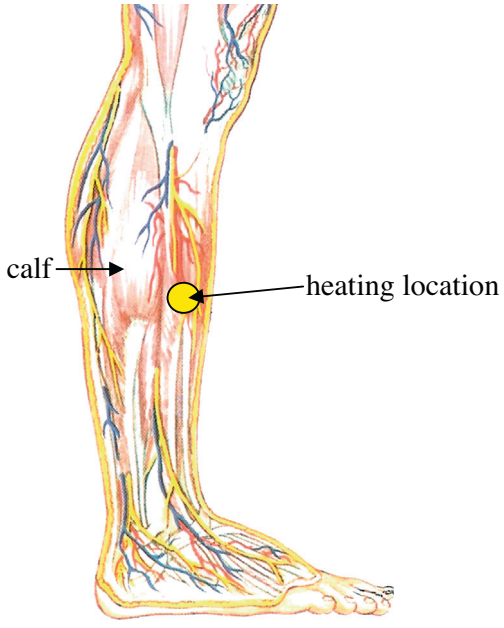

Fig. 1. Schematic of the calf and the heating location [21].

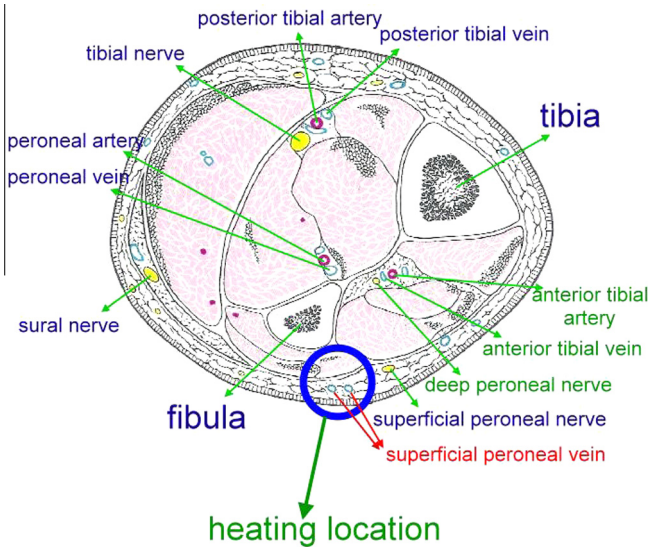

Fig. 2. The axial image of the right leg [15] containing the heating location and the two superficial peroneal veins.

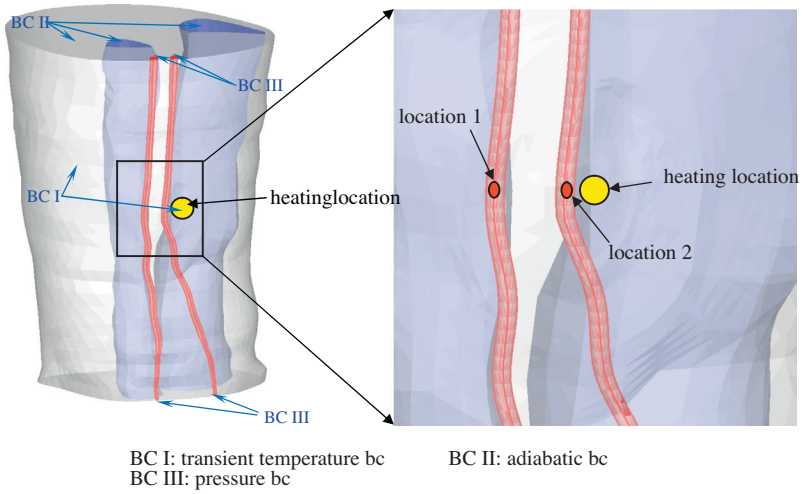

Fig. 3. Schematic of the calf section around the heating location and the specified boundary conditions.

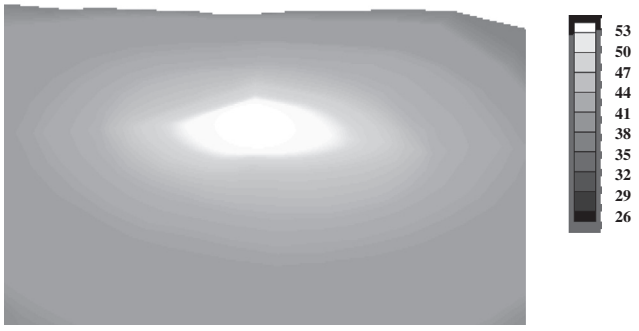

Fig. 4. The temperature contours measured by the real time IR camera.

Table 1
Summary of the employed coefficients and the prescribed temperatures in the current simulation.

K	$0.840419 + 0.001403T$ W/m °C	Thermal conductivity
C_p	3,594 J/kg °C	Specific heat of tissue
M	$\mu(T^0C) = 0.0021\left\{1 - 4\frac{T-37}{T+273}\right\}$ kg/ms	Viscosity of blood
ρ_c	1,035 kg/m^3	Density of calf
ρ_b	1,035–0.41335(T-310) kg/m^3	Density of blood
T_E	22 °C	Environment temperature

denotes the specific enthalpy of the blood and C_p is the specific heat at the constant pressure. The vector $\underline{q}$ denotes the diffusive energy flux defined as $\underline{q} = k\nabla T$, where T is the blood temperature and k is the thermal conductivity.

In addition to the above set of Eqs. ((1)–(3)) applied in the blood vessel shown in Fig. 3, the diffusion-type Pennes bioheat equation [17] given below is employed to model the transfer of heat in perfused tissues

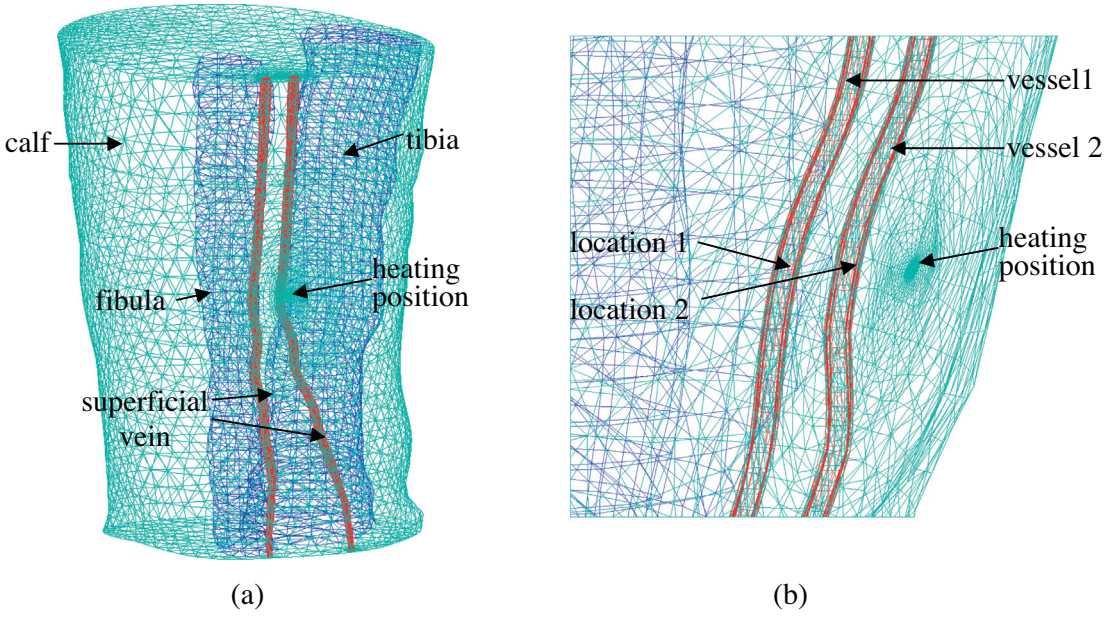

Fig. 5. (a) The surface meshes generated in the investigated calf section; (b) The zoom-in area around the heating position.

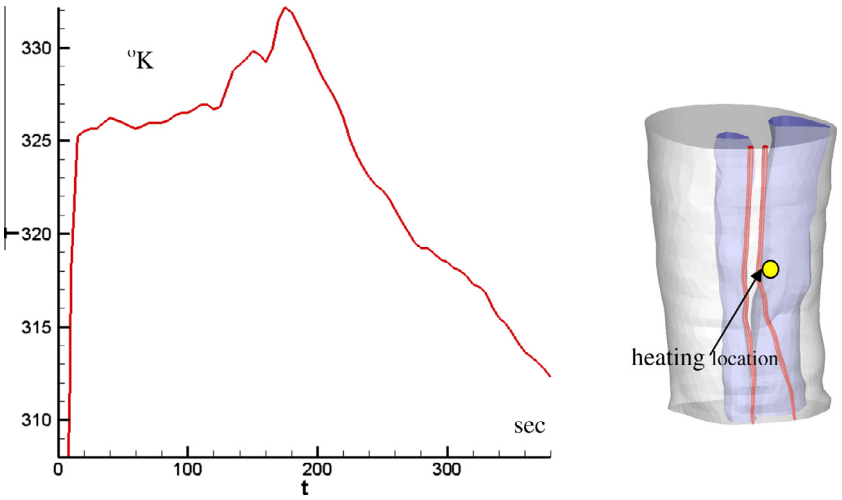

Fig. 6. The temperature measured at the heating position on skin surface is plotted with respect to time.

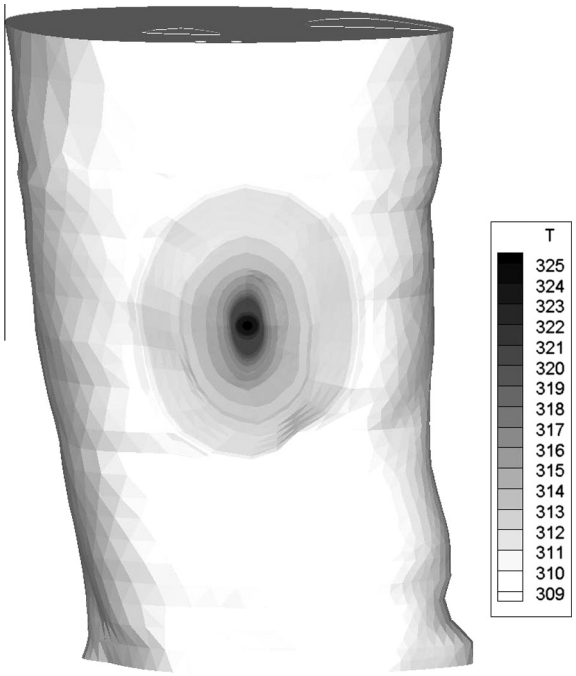

Fig. 7. The predicted contours of the skin surface temperature.

$$\rho_t C_t T_t = k_t \nabla^2 T - W_b C_p (T - T_\infty). \quad (4)$$

In this energy conservation equation applied to tissues, ρ_t, C_t and k_t denote, respectively, the density, specific heat, and thermal conductivity of the tissues under investigation. In the last term on the right hand side of Eq. (4), T_∞ denotes the temperature at a remote location and W_b is known as the perfusion rate for the tissue cooling. For simplicity, the value of W_b is assumed to be 0.5 kg/m^2.

Eq. (4) will be solved together with the hemodynamic equations ((1)–(3)) by employing the commercial software CFD-ACE$^+$ [18]. This finite volume package includes the CFD-GEOM modulus for easily generating a structured type surface mesh. Subject to these surface mesh points, the solution domain is divided into a number of cells known as control volumes. The governing equations shown above are numerically integrated over each of these computational cells using the modulus for solving the dependent variables which are stored at cell centers. Third-order accurate upwinding scheme is applied to approximate advection terms, while the diffusion terms are approximated by the second-order space-centered scheme and the time differencing is first-order accurate by employing backward Euler scheme. An advanced multigird solver is chosen in this study to effectively calculate the velocity and enthalpy respectively from the discretized equations for (2) and (3).

In Eqs. ((1)–(3)), these is no governing equation for the field variable p. As a result, the pressure-based method, which utilizes the continuity equation to formulate one equation for the pressure, is employed in this study. In the current segregated approach, the pressure–velocity coupling is accomplished for the momentum equations for $\underline{u}$ and the continuity equation for p via the SIMPLE C (Semi-Implicit Method for Pressure-Linked Equation Consistent) iterative solution algorithm. A graphical user interface (GUI) and the CFD-VIEW modulus are both available for us to easily specify the physical properties, which are also stored at cell centers, shown in the equations and to clearly visualize the simulated results.

The boundary conditions applied at the calf section of the first author's leg are shown in Fig. 3. The notation BC I represents the transient temperature boundary condition, where the time dependent data are measured experimentally using the real time IR camera. The measured temperature plotted in Fig. 4 will be used as our input boundary condition to solve the energy equation (4) in tissues. BC II is designed as the adiabatic boundary condition. At the interface separating the blood vessels and their surrounding tissues, thermal energy balance between the Fourier law of conduction and the Newtonian law of cooling is applied. One can also simplify the derivation of interface condition by neglecting the convection cooling near the blood vessel. As a result, only the energy balance of heat conduction from the tissue and blood vessel sides is considered. In CFD-ACE$^+$ the interface condition has been automatically imposed without the need of user's specification. BC III denotes the inlet and outlet boundary conditions for the blood flow equations. At these two truncated planes, they are specified with the fixed pressure values.

A hybrid grid containing the structured- and unstructured-type meshes is shown in Fig. 5. A total number of 15,371 nodal points is generated. These mesh points have been properly distributed so that the predicted solutions can more faithfully represent the physical phenomenon of the problem under current investigation. In all investigations, calculation of the enthalpy over one time increment will be terminated when the residual norm falls below 10^{-15}. By increasing the number of nodal points (15,371 nodal points) by an amount of 50% (or 23,171 nodal points), only a neg-

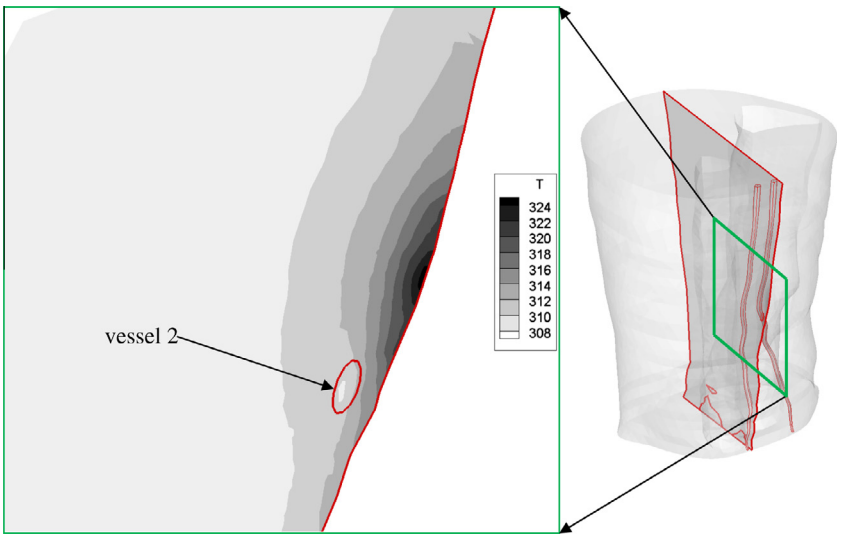

Fig. 8. The predicted temperature contours on the cutting plane that contains the heating location. The temperature has a smaller value near the vessel 2.

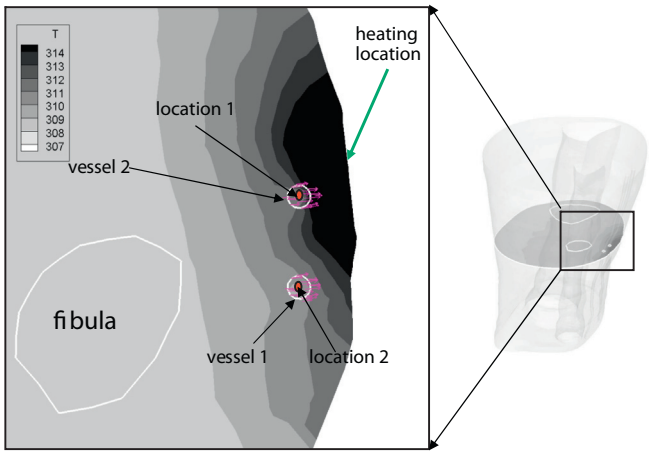

Fig. 9. The predicted temperature contours on the cutting plane that contains the location 1, location 2 and heating location. The temperatures are smaller near the vessels 1 and 2.

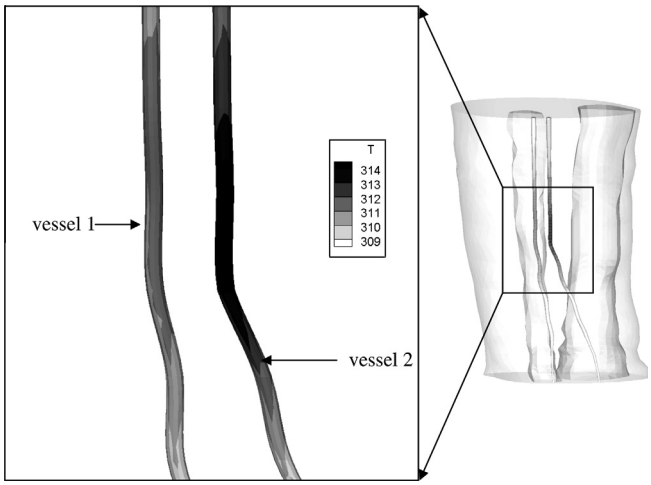

Fig. 10. The predicted temperature on the vessel surfaces.

ligibly small difference is observed in the simulated results. On the contrary, when the number of mesh points is decreased by 50% (or 7,403 nodal points), the computed difference becomes apparent. Hence the mesh generated by 15,371 nodal points will be employed in the present simulation study.

In order to know the temperature distribution due to a burning moxa, in this measurement the IR image is recorded under an almost dark condition. The camera and the subject under investigation are both apart from the external IR source. The room temperature and the relative humidity are maintained at the fixed values of 22 ± 0.1 °C and 60 ± 7%, respectively. Thermography has been carried out with a calibrated IR camera (Electrophysics TVS-500 EX system), which is equipped with a 3.5" transflective color LCD monitor. Sensitivity, accuracy, and resolution of the employed camera are kept at the values of 0.06 °C, ±2 °C and 1.68 mrad, respectively. The distance between the camera and the subject under investigation is chosen to be 0.3 m. The infrared images of the subject obtained at a sampling rate of 4 Hz are directly recorded in the PC hard disk.

3. Results and discussion

The specific heat and density of tissues of the investigated calf section are denoted as C_t and ρ_t, respectively. At the normal state, these coefficients are prescribed respectively as $C_t = 3{,}594$ J/kg °C [19] and $\rho_t = 1{,}035$ kg/m^3. The thermal conductivity of human tissues is assumed to change with the temperature (T) according to $k_t = 0.840419 + 0.001403T$ W/m °C [20]. The rest of the employed coefficients for the material properties are tabulated in Table 1.

The temperature on the skin surface is controlled to be lower than 60 °C, which is about the highest temperature that human skin can endure, to avoid scarring. Fig. 6 shows the time varying temperature at the heating position of skin surface. The pressures at the inlet and outlet boundaries of the blood vessels are specified at 50 N/m^2 and 0 N/m^2, respectively. The temperature at the rest of the boundary is specified at 35 °C. The predicted temperature on the skin surface is shown in Fig. 7.

When the skin surface is heated by a burning moxa, the resulting higher tissue temperature can cause mast cells to degranulate. Such a degranulation of cells helps to increase the hydraulic pressure of capillaries and the permeability of capillaries. The effect of moxibustion can therefore enhance Chi-blood circulation. Fig. 8 shows the predicted temperature contours on the cutting plane

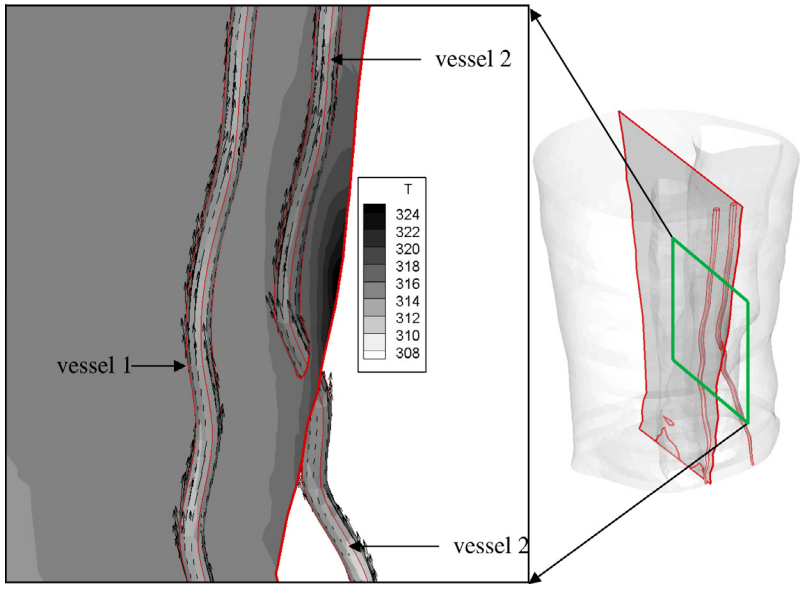

Fig. 11. The predicted velocity vectors in the vessels, and the temperature contours on the cutting plane that contains the heating location.

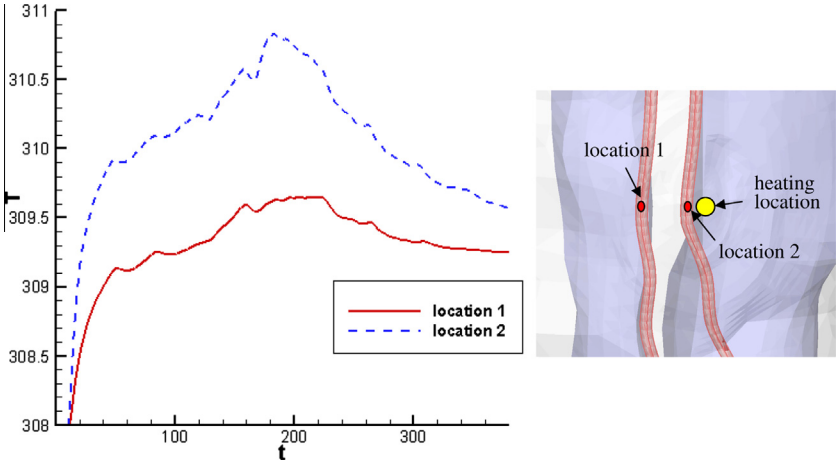

Fig. 12. The predicted time-varying temperatures at the locations 1 and 2. Locations 1 and 2 are at the center positions of vessels 1 and 2.

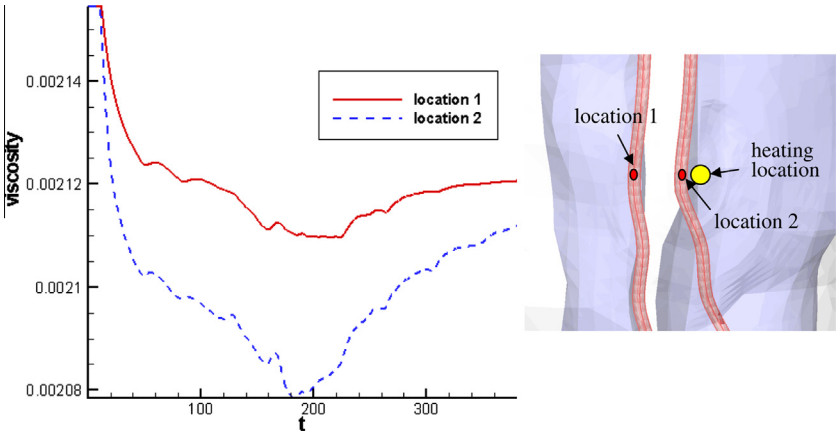

Fig. 13. The blood viscosities are plotted with respect to time at the locations 1 and 2. Locations 1 and 2 are at the center positions of vessels 1 and 2.

of the calf that contains the heating position. From this Figure the transfer of heat from skin surface to tissues and blood vessels can be seen. The temperature is also found to be lower around the vessels that are on the right bottom side of Fig. 8. This phenomenon

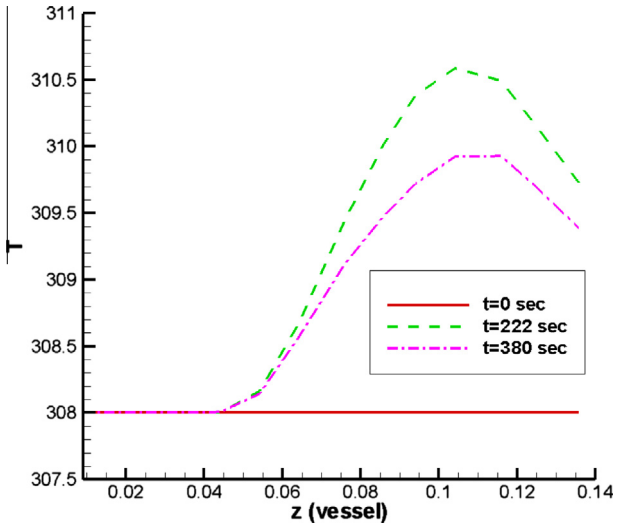

Fig. 14. The predicted temperatures $T(z, t)$ at the center position of the blood vessel 1 at $t = 222$ s and 380 s.

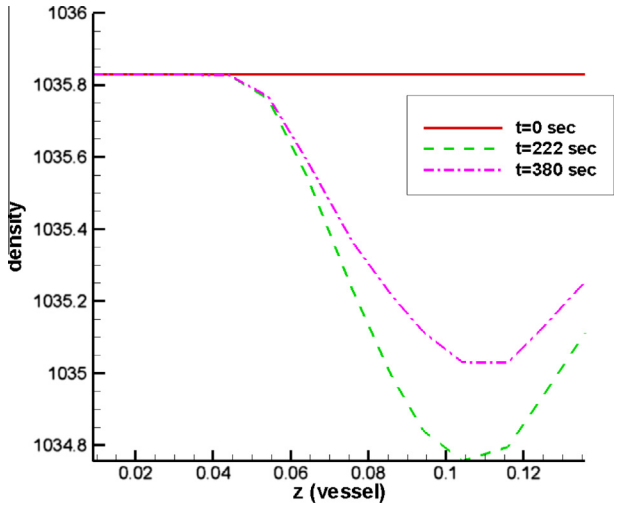

Fig. 16. The predicted density $\rho(z, t)$ at the center position of the blood vessel 1 at $t = 222$ s and 380 s.

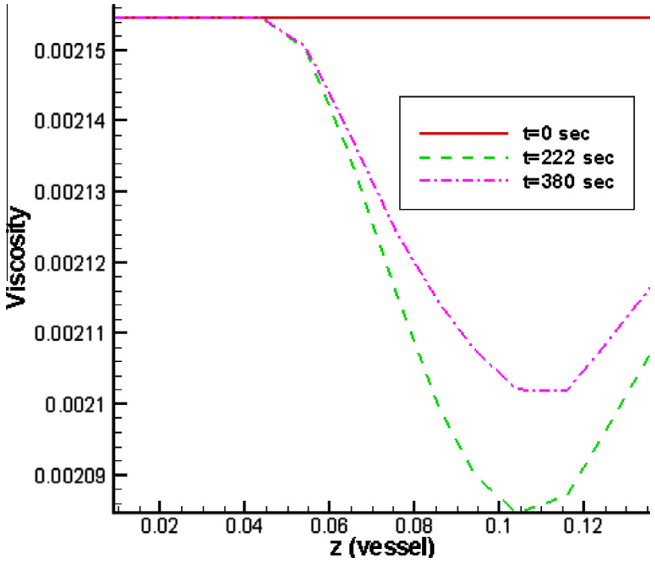

Fig. 15. The predicted viscosity $\mu(z, t)$ at the center position of the blood vessel 1 at $t = 222$ s and 380 s.

can be also observed in Fig. 9, which plots the predicted temperature contours on the cutting plane of the calf that passes the position where the moxa is placed. The temperature has a lower value around the blood vessels.

The predicted temperature on the vessel surface is shown in Fig. 10. Both of the velocity vectors inside the blood vessels and the predicted temperature contours on the cutting plane that contains the moxibustion location are shown in Fig. 11 at $t = 194$ s. It is seen that the speed of blood flow is faster at a time when reaching the heating area. Such a flow acceleration results from the decreased blood viscosity in the sense that the Reynolds number becomes larger. The time-varying temperature and the viscosity of the blood flow shown, respectively, in Figs. 12 and 13 at the locations 1 and 2 indicate that a lower viscosity corresponds to a higher temperature.

Along the vessel 1, the temperatures are plotted from the bottom to the top in Fig. 14 at $t = 0$, 222, 380 s. At $t = 222$ s, the temperature reaches its maximum magnitude at $z = 0.06$ m–0.10 m (heating position is at $z = 0.08$ m). In Figs. 15 and 16, one can also observe that the predicted higher temperature is the result of the lower viscosity and density.

Moxibustion has enjoyed widespread popularity in Chinese medicine treatments. No information is, however, available for the time being for us to know more precisely the amount of heat that has been transferred to the body during the heating process. To provide some scientific and useful heat flux, the surface temperature on the skin measured by IR camera is used as the boundary condition to perform heat and fluid flow simulations. The time-varying heat flux and total heat transfer from skin to human body generated by the burning moxa is shown in Fig. 17. The transfer of heat during the whole moxibustion process will be illustrated by plotting the predicted moxibustion heat.

When performing moxibustion, it is interesting to know whether or not a standing pose is more effective than a lying pose. Two simulations with the gravity effect along z (simulating the standing pose) and y directions (simulating the lying pose) are therefore carried out. In Fig. 18, one can find that the mean velocity under the lying pose is always larger than the velocity predicted under the standing pose. The reason is that the blood flow can return back more easily to the heart without the effect of gravity. However, in standing pose, when the temperature is higher the buoyancy force will accelerate blood flow. Therefore, standing pose has a larger change of the mean velocities tabulated in Table 2.

4. Conclusions

In the present study, the increased skin surface temperature during moxibustion has been obtained experimentally from the real time IR measurement. Based on this experimental measurement of the surface temperature, beneath the skin the distribution of surface temperature can be numerically simulated. When the temperature is increased, blood flow is found to increase because of the decreased blood viscosity. The difference between the lying and standing poses during moxibustion is also numerically studied. Under the lying pose, the blood flow is found to have a larger mean velocity magnitude while the standing pose has a larger mean velocity change. Through this study, we know that the lying pose is considered to be a more effective choice when practicing the moxibustion since a larger blood flow speed can transfer heat more quickly to the whole body.

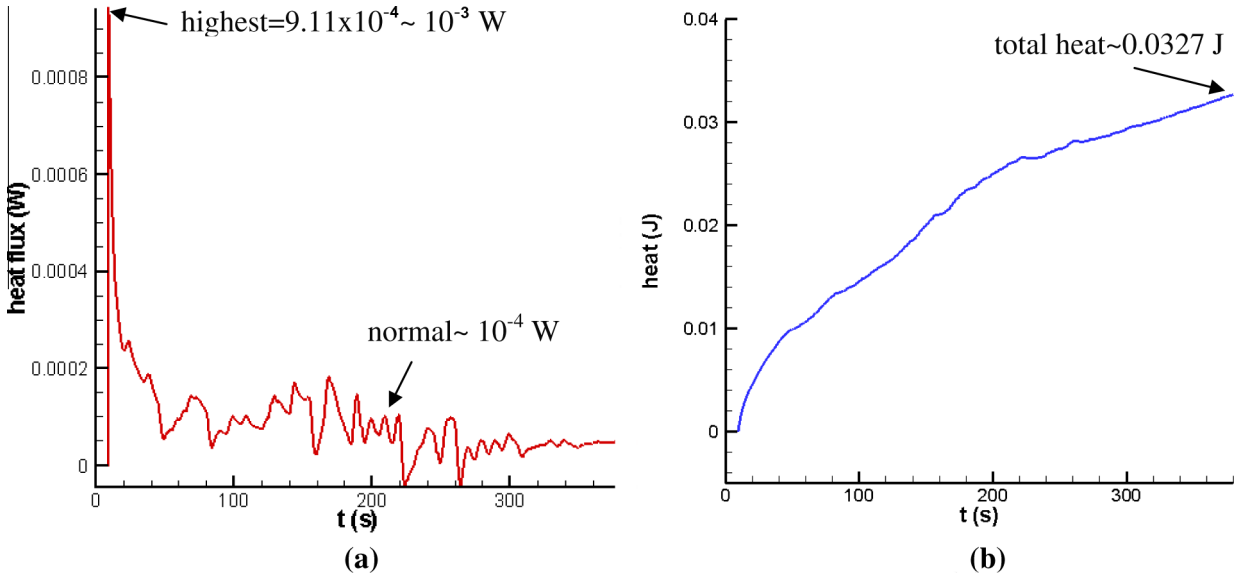

Fig. 17. The predicted time-varying (a) heat flux and (b) total heat from the skin to the body generated by the burning moxa.

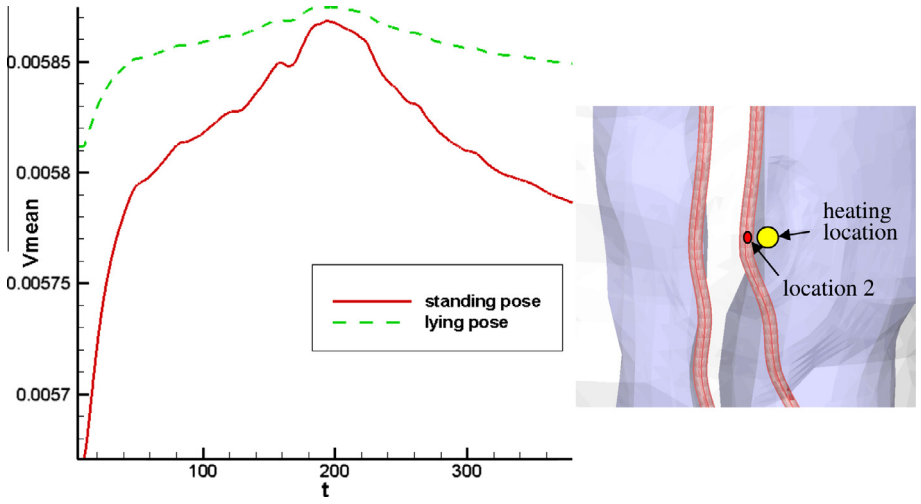

Fig. 18. The predicted mean velocities, which are plotted with respect to time at the location 2, under two different body poses.

Table 2
Comparison of the mean velocities between the blood vessels 1 and 2 before and at a time subject to moxibustion.

	V_{mean} in vessel 1 under lying pose	V_{mean} in vessel 2 under lying pose	V_{mean} in vessel 1 under standing pose	V_{mean} in vessel 2 under standing pose
Before moxibustion	5.96187×10^{-3} 0 s (100%)	5.81148×10^{-3} 0 s (100%)	5.81950×10^{-3} 0 s (100%)	5.67088×10^{-3} 0 s (100%)
Under moxibustion	6.00023×10^{-3} 222 s (100.643%)	5.87232×10^{-3} 194 s (101.05%)	5.94355×10^{-3} 222 s (102.132%)	5.86833×10^{-3} 194 s (103.482%)

Acknowledgments

The authors will acknowledge their thanks to Prof. Wen-Pin Shih who provided us the Electrophysics TVS-500 EX system to perform temperature measurement.

References

[1] S. Maruyama, S. Takashima, H. Takeda, J. Okajima, A. Komiya, T. Seki, T. Yambe, Study on bio-heat transfer in living body by using abdominal heating controller, in: Proceeding of 44th National Heat Transfer, Symposium, 2007.

[2] G. Brix, M. Seebass, G. Hellwig, J. Griebel, Estimation of heat transfer and temperature rise in partial-body regions during MR procedures: an analytical approach with respect to safety considerations, Magn. Reson. Imaging 20 (2002) 65–76.

[3] J.W. Durkee Jr., P.P. Antich, Exact solutions to the multi- region time-dependent bioheat equation with transient heat sources and BCs, Phys. Med. Biol. 36 (3) (1991) 345–368.

[4] T.W.H. Sheu, M.A. Solovhuk, A.W.J. Chen, M. Thiriet, On an acoustics–thermal-fluid coupling model for the prediction of temperature elevation in liver tumor, Int. J. Heat Mass Transfer 54 (17–18) (2011) 4117–4126.

[5] M.A. Solovchuk, T.W.H. Sheu, W.L. Lin, I. Kuo, M. Thiriet, Simulation study on acoustic streaming and convective cooling in blood vessels during a high-intensity focused ultrasound thermal ablation, Int. J. Heat Mass Transfer 55 (4) (2012) 1261–1270.

[6] W. Shen, J. Zhang, Skin thermal injury prediction with strain energy, Department of Computer Science, Technical Report, No. 427–05, KY, USA, University of Kentucky, 2005.
[7] F.C. Henriques, A.R. Moritz, Studies of thermal injuries I. The conduction of heat to and through skin and the temperatures attained therein; a theoretical and an experimental investigation, Am. J. Pathol. 23 (1947) 531–549.
[8] A.M. Stoll, Thermal properties of human skin related to nondestructive measurement of epidermal thickness, J. Invest. Dermatol. 69 (1977) 328–332.
[9] A.M. Stoll, M.A. Chianta, J.R. Piergallini, Thermal conduction effects in human skin, Aviat. Space Environ. Med. 50 (1979) 778–787.
[10] G.T. Anderson, G. Burnside, A noninvasive technique to measure perfusion using a focused ultrasound heating source and a tissue surface temperature measurement, in: Advances in Measuring and Computing Temperatures in Biomedicine, The Winter Annual Meeting of ASME, vol. 147, Dallas, Texas, 1990, pp. 31–35.
[11] L. Fei, Researches and developments of meridian physical basic and function experiments, Chin. Sci. Bull. 43 (6) (2000) 658–672.
[12] T.W.H. Sheu, V.C. Huang, Development of an electro osmotic flow model to study the dynamic behavior in human meridian, Int. J. Numer. Methods Fluids 56 (2008) 739–751.
[13] V.C. Huang, T.W.H. Sheu, On a dynamical view on the meridian transmission, J. Accord Integrative Med. 4 (2) (2008) 97–107.
[14] V.C. Huang, T.W.H. Sheu, Tissue fluids in microchannel subjected to an externally applied electric potential, Int. J. Numer. Methods Heat Fluid Flow 19 (1) (2009) 64–77.
[15] J.K. Yang, Meridian Cross-section Anatomy, Shang Hai Science Technology Press (1997) 76.
[16] Z.P. Shul'man, V.A. Mansurov, Determination of the rheological properties of whole blood by the nonstationary method of pulsed changing of the rate of shear, J. Eng. Phys. Thermophys. 78 (5) (2005) 1018–1021.
[17] H.H. Pennes, Analysis of tissue and arterial blood temperature in the resting human forearm, J. Appl. Physiol. 11 (2) (1948) 93–122.
[18] CFD-ACE-GUI User Manual Volume II, CFD Research Corporation, 2003, pp. 85–94.
[19] A.S.T. Blake, G.W. Petley, C.D. Deakin, Effects of changes in packed cell volume on the specific heat capacity of blood: implications for studies measuring heat exchange in extracorporeal circuits, Br. J. Anaesth. 84 (1) (2000) 28–32.
[20] T. Murat, C. Unal, P. Cem, The bio-heat transfer equation and its applications in hyperthermia treatments, Eng. Comput. 23 (4) (2006) 451–463.
[21] K.W. Chang, Meridian Anatomy, Zhi-Yang Press, 1999, p. 47.